scientific reports

OPEN

MHD Casson carbon nanotube flow with mass and heat transfer under thermosolutal Marangoni convection in a porous medium: analytical solution

A. B. Vishalakshi[1], U. S. Mahabaleshwar[1] & M. Hatami[2]✉

Current work portrays the flow of Marangoni convection Magneto hydrodynamics Casson fluid with carbon nanotubes under the effect of transpiration and radiation. The carbon nanotube particles namely water-single wall carbon nanotubes are inserted in the fluid to enhance better thermal efficiency. This type of flow problems is applicable for real life situations such as drying of silicon wafers, glues, crystal growth and heat exchangers and so on. The ordinary differential equations (ODEs) form of the result is yield to convert partial differential equations of the given equation by using similarity variables. Then this resulting ODEs are solved analytically, firstly using momentum equation to get solution domain and then by using this domain the energy equation solved to get the temperature profile in terms of Laguerre polynomial. Additionally, mass transpiration is also solved to get the concentration profile in terms of Laguerre polynomial. By using the different controlling parameters, the results can be discussed. And the effect of this parameters are discussed by using graphical arrangements. The newness of the present work is to explain the physically flow problem on the basis of chemically radiative thermosolutal Marangoni convective fluid.

Abbreviations

B. Cs	Boundary conditions
MHD	Magneto hydrodynamics
ODE	Ordinary differential equation
PDE	Partial differential equation

List of symbols

B_0	Strength of uniform magnetic field (Tesla)
C	Concentration of the fluid $\left(\mathrm{mol\,m^{-3}}\right)$
C_∞	Concentration of the fluid at infinity $\left(\mathrm{mol\,m^{-3}}\right)$
C_w	Concentration at wall $\left(\mathrm{mol\,m^{-3}}\right)$
C_P	Specific heat at constant pressure $\left(\mathrm{J\,Kg^{-1}\,K^{-1}}\right)$
D	Mass diffusivity $\left(\mathrm{m^2\,S^{-1}}\right)$
Da^{-1}	Inverse Darcy number
G	Chemical reaction parameter
I	Heat source/sink parameter
K	The permeability of porous medium $\left(\mathrm{m^2}\right)$
L	Characteristic length
Q	Chandrasekhar's number
Q_0	Heat source/sink coefficient

[1]Department of Mathematics, Davangere University, Shivagangotri, Davangere 577007, India. [2]Mechanical Engineering Department, Ferdowsi University of Mashhad, Mashhad, Iran. ✉email: m-hatami@um.ac.ir; m.hatami@xjtu.edu.cn

q_r	Radiative heat flux
T_∞	Free stream temperature (K)
T	Temperature of the fluid (K)
(u, v)	Components of velocities $\left(\mathrm{ms}^{-1}\right)$
V_0	Mass transfer velocity $\left(\mathrm{ms}^{-1}\right)$

Greek symbols

α_r	Mean absorption coefficient
β	Solution domain
ϕ	Concentration profile
μ	Dynamic viscosity $\left(\mathrm{m}^2\,\mathrm{s}^{-1}\right)$
θ	Temperature profile
κ	Thermal conductivity (W/mK)
σ	Electrical conductivity $\left(\mathrm{Sm}^{-1}\right)$
σ_0	Equilibrium surface tension
σ^*	Stefan-Boltzmann constant $\left(\mathrm{Wm}^{-2}\,\mathrm{K}^{-4}\right)$
ρ	Density of the fluid $\left(\mathrm{kg\,m}^{-3}\right)$

Subscripts

∞	Free stream condition
η	Differentiation with respect to η

Basically in the interfaces of liquid–liquid or liquid–gas we found the layers of Marangoni convection, these layers are normally called as dissipative layers and these layers plays a great role in industrial applications. Gibbs[1] discovered this phenomenon in last century. Napolitano[2,3] addressed the original work of this field. Temperature and concentration dependent surface tension is respectively called as Thermocapillary and destillocapillary effects[4,5]. The application of Marangoni convection can be found in the fields of crystal growth, soap films and crystal growth. Chamkha et al.[6] worked on Marangoni convection problem and he come to concluded that surface driven flows may build layers along the interfaces as well as buoyancy effect brought on by gravity and the external pressure gradient. When employing the arc length as coordinates, Napolitano et al.[7] addressed the issue that non-Marangoni boundary layers in bulk fluids do not explicitly depend on the geometry of the interface. Only a few research and initiatives have been made to comprehend the fundamental laws of nature and the issues surrounding Marangoni convection.

The magnetohydrodynamics thermosolutal Marangoni convection over a flat surface in the presence of a heat source/sink parameter was addressed by Mudhaf and Chamkha[8]. The effects of heat transmission on MHD and radiation are examined by Aly and Ebaid[9]. Marangoni boundary layer nanofluid led him to conclude that a magnetic parameter causes a fluid's velocity to slow down and its temperature to rise. The double-diffusive convection in an open cavity was studied by Arbin et al.[10] Nayak[11] investigated the magnetohydrodynamics viscoelastic fluid under the impact of chemical reaction effect with porous medium. See some other examples related to Marangoni convection are seen in[12–15].

Recent advancements in nanotechnology helps to conduct innovative techniques to develop applications of nanofluids in many fields. The term nanofluid is initially addressed by Choi[16]. Arshad et al.[17–20] investigated flow problems in the presence of different nanofluids with various aspects such as heat source/sink parameter, radiation and so on. See some more references on nanofluid in[21,22]. Similarly, carbon nanotubes take a lot of attention in many fields such as chemistry, physics, medicine, biology, and Engineering. These are the few examples for the importance of nanofluids in many fields[23–25]. Additionally, the fluid known as Casson fluid is quite interesting, and it is used to describe non-Newtonian phenomena. The researcher Casson addressed this flow model in 1995. This flow model is useful in many real life applications. See some of the recent works of this model in[26–28].

Effect of Porous medium and thermal radiation take places major role in the fluid flow because these effects in the fluid flow is used in many industrial and real life applications namely metallurgic processes, geophysical and allied areas[29]. There are many equations and derivations are available to describe the fluid flow process through porous medium and also the effect of thermal radiation. See some more articles published on porous medium and thermal radiation are given in [30–32].

The current study is investigating Casson fluid flow in the presence of carbon nanotubes with thermal radiation and mass transpiration. It is prompted by the aforementioned studies. In this problem we use the new method to provide a similarity variable on the impact of chemically radiative thermosolutal Marangoni convective fluid flow, the partial differential equations of the governing equations are converted into ordinary differential equations. The novelty of the present work explains that the momentum energy and mass equation solved analytically to get the solution domain and the solution in terms of Laguerre polynomial. The impact of different parameters is examined with the help of graphical scenario. This work is also important in many industrial applications such as welding machines, metallurgical process, geosciences, space technology and so on. The current issue is persuasively argued in the work of Mahabaleshwar et al.[33].

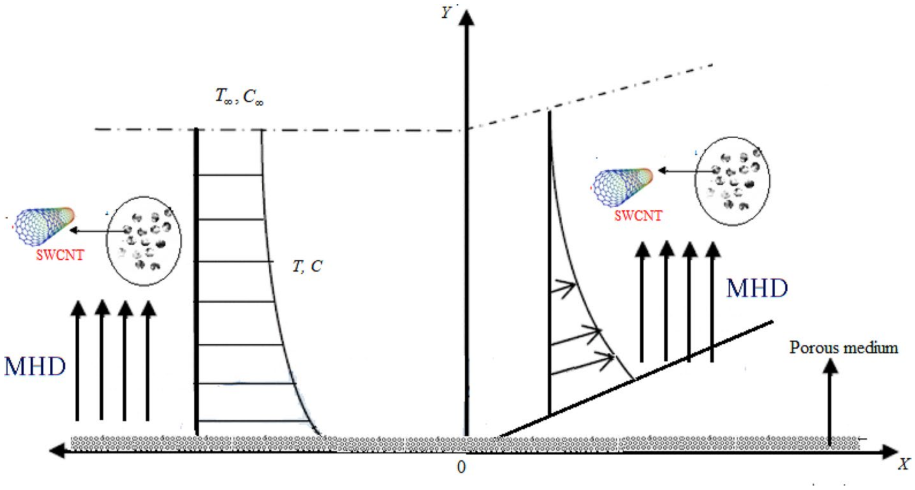

Figure 1. Schematic diagram of the Casson fluid flow.

Mathematical formulation and solution

Flow of a Casson fluid with thermosolutal Marangoni convection thermal radiation and transpiration is analyzed in this study. The particles of carbon nanotubes are immersed inside the fluid to get better thermal efficiency. Temperature gradients and solute concentrations define surface tension. Figure 1 shows a schematic representation of fluid flow.

Let us assume the surface of the fluid move towards x axis. The governing equations can be defined as follows by taking into account the aforementioned premises (See[34,35]).

$$\frac{\partial u}{\partial x}+\frac{\partial v}{\partial y}=0, \tag{1}$$

$$u\frac{\partial u}{\partial x}+v\frac{\partial v}{\partial y}=\nu_{nf}\left(1+\frac{1}{\Lambda}\right)\frac{\partial^2 u}{\partial y^2}-\left(\frac{\mu_{nf}}{\rho_{nf}K}+\frac{\sigma_{nf}B_0^2}{\rho_{nf}}\right), \tag{2}$$

$$\begin{aligned}u\frac{\partial T}{\partial x}+v\frac{\partial T}{\partial y}=&\frac{\kappa_{nf}}{(\rho C_P)_{nf}}\frac{\partial^2 T}{\partial y^2}+\frac{\mu_{nf}}{(\rho C_P)_{nf}}\left(\frac{\partial u}{\partial y}\right)^2+\left(\frac{\mu_{nf}}{(\rho C_P)_{nf}K}+\frac{\sigma_{nf}B_0^2}{(\rho C_P)_{nf}}\right)u^2\\&-\frac{1}{(\rho C_P)_{nf}}\frac{\partial q_r}{\partial y}+\frac{Q_0}{(\rho C_P)_{nf}}(T-T_\infty),\end{aligned} \tag{3}$$

$$u\frac{\partial C}{\partial x}+v\frac{\partial C}{\partial y}=D\frac{\partial^2 C}{\partial y^2}-G(C-C_\infty), \tag{4}$$

Here the Casson fluid term is used for characterize the non-Newtonian fluid. Magnetic term and porous medium term is used for many scientific and technological phenomena. Effect of Porous medium and thermal radiation take places major role in the fluid flow because these effects in the fluid flow is used in many industrial and real life applications. Heat source/sink in the fluid flow influences the characteristics of heat transfer as there is a substantial amount of difference in the temperature between the surface and the fluid. Also the combination of mass transfer and heat source/sink helps in overcoming the problem of boundary layer separation.

The surface tension along with heat and mass boundaries is given by (See[36–38])

$$\sigma=\sigma_0[1-\gamma_T(T-T_\infty)-\gamma_C(C-C_\infty)], \tag{5}$$

Coefficients of surface tension respectively for heat and mass is given by

$$\gamma_T=-\frac{1}{\sigma_0}\left(\frac{\partial\sigma}{\partial T}\right)_T,\quad\text{and}\quad\gamma_C=-\frac{1}{\sigma_0}\left(\frac{\partial\sigma}{\partial C}\right)_T. \tag{6}$$

The terms from Eqs. (1–6) are specified in this section under Nomenclature.

Associated B. Cs

$$\mu\left(\frac{\partial u}{\partial y}\right)_{y=0}=-\left(\frac{\partial\sigma}{\partial x}\right)_{y=0}=\sigma_0\left(\gamma_T\left(\frac{\partial T}{\partial x}\right)_{y=0}+\gamma_C\left(\frac{\partial C}{\partial x}\right)_{y=0}\right), \tag{7}$$

$$\left.\begin{array}{ll} V(x,0) = V_0, & u(x,\infty) = 0 \\ T(x,0) = T_\infty + T_0 X^2, & T(x,\infty) = T_\infty \\ C(x,0) = C_\infty + C_0 X^2, & C(x,\infty) = C_\infty \end{array}\right\}. \tag{8}$$

here $X = \frac{x}{L}$, and $L = -\frac{\mu\nu}{\sigma_0 T_0 \gamma_T}$ is the characteristic length, T_0 and C_0 are constants. In addition, the following transformations are defined.

$$\left.\begin{array}{l} \psi\left(x,y\right) = \nu X f(\eta) \quad \eta = \frac{y}{L} \\ T\left(x,y\right) = T_\infty + T_0 X^2 \theta(\eta) \\ C = C_\infty + C_0 X^2 \phi(\eta) \end{array}\right\}, \tag{9}$$

By using dimensional form of velocity components are given by

$$u = \frac{\nu}{L} f_\eta(\eta), \quad v = -\frac{\nu}{L} f(\eta). \tag{10}$$

The value q_r can be defined on the basis of Rosseland's approximation as follows (See[39–42].

$$q_r = -\frac{4\sigma^*}{3\alpha_r}\frac{\partial T^4}{\partial y}, \tag{11}$$

where the ambient temperature T^4 expands in terms of the Taylor's series as

$$T^4 = T_\infty^4 + 4T_\infty^3(T - T_\infty) + 6T_\infty^2(T - T_\infty)^2 + \cdots \tag{12}$$

when the higher order elements in this equation are ignored, this results in

$$T^4 \cong 3T_\infty^3 + 4T_\infty^3 T. \tag{13}$$

On applying Eq. (8) into Eq. (6), then the first order derivative of heat flux can be given by

$$\frac{\partial q_r}{\partial y} = -\frac{16\sigma^* T_\infty^3}{3\alpha_r}\frac{\partial^2 T}{\partial y^2}. \tag{14}$$

Therefore, the Eq. (3) can b rewritten as

$$\begin{aligned} u\frac{\partial T}{\partial x} + v\frac{\partial T}{\partial y} = \frac{\kappa_{nf}}{(\rho C_P)_{nf}}\frac{\partial^2 T}{\partial y^2} + \frac{\mu_{nf}}{(\rho C_P)_{nf}}\left(\frac{\partial u}{\partial y}\right)^2 + \left(\frac{\mu_{nf}}{(\rho C_P)_{nf} K} + \frac{\sigma_{nf} B_0^2}{(\rho C_P)_{nf}}\right)u^2 \\ + \frac{1}{(\rho C_P)_{nf}}\frac{16\sigma^* T_\infty^3}{3k^*}\frac{\partial^2 T}{\partial y^2} + \frac{Q_0}{(\rho C_P)_{nf}}(T - T_\infty). \end{aligned} \tag{15}$$

By using Eqs. (9) and (10) in Eqs. (2) and (3) to get

$$\varepsilon_1\left(1 + \frac{1}{\Lambda}\right)f_{\eta\eta\eta} + \varepsilon_2\left(ff_{\eta\eta} - f_\eta^2\right) - \left(\varepsilon_1 Da^{-1} + \varepsilon_3 Q\right)f_\eta = 0, \tag{16}$$

$$(\varepsilon_5 + R)\theta_{\eta\eta} + \Pr\varepsilon_4\left(f\theta_\eta + \left(I - 2f_\eta\right)\theta\right) + Ec\left(\varepsilon_1 f_{\eta\eta}^2 + \left(\varepsilon_1 Da^{-1} + \varepsilon_3 Q\right)f_\eta\right) = 0, \tag{17}$$

$$\phi_{\eta\eta} + Sc\left(f\phi_\eta - \left(\delta + 2f_\eta\right)\phi\right) = 0, \tag{18}$$

the B. Cs reduces to

$$\begin{array}{l} f(0) = V_C, \ \ f_\eta(\infty) = 0, \quad f_{\eta\eta}(0) = -2(1 + M_a) \\ \theta(0) = 1, \ \ \theta(\infty) = 0, \ \ \phi(0) = 1, \ \ \phi(\infty) = 0, \end{array} \tag{19}$$

here $V_C = -\frac{\gamma}{L}\mathrm{v}_0$ is the mass transpiration, here $V_C = 0$, $V_C > 0$ and $V_C < 0$ respectively indicates suction, injection and no-permeability cases. $\Pr = \frac{\kappa}{\mu C_P}$, $Sc = \frac{\nu}{D}$ and $\delta = \frac{GL^2}{\nu}$ respectively indicates the Prandtl number, Schmidt number, chemical reaction coefficient. $R = \frac{16\sigma^* T_\infty^3}{3\alpha_r \kappa}$ is the radiation number, $I = \frac{Q_0 L^2}{\varepsilon_4 \rho C_P \nu}$ is the heat source or sink parameter, $Da^{-1} = \frac{L^2}{K}$ is inverse Darcy number, $Q = \frac{\sigma B_0^2 L^2}{\rho\nu}$ is Chandrasekhar's number, $Ec = \frac{\gamma^2}{L^2 T_0 C_P}$ is Eckert number, and finally $Ma = \frac{Ma_C}{Ma_T}$ is the Marangoni number (Thermosolutal surface tension ratio), $Ma_C = \frac{\sigma_0 \gamma_C C_0 L C_P}{\kappa}$ and $Ma_T = \frac{\sigma_0 \gamma_T T_0 L C_P}{\kappa}$ are the solutal and thermal Marangoni numbers. Carbon nanofluid quantities used in Eqs. (16) and (17) can be defined as (See[43,44])

$$\varepsilon_1 = \frac{\mu_{nf}}{\mu_f}, \ \varepsilon_2 = \frac{\rho_{nf}}{\rho_f}, \ \varepsilon_3 = \frac{\sigma_{nf}}{\sigma_f}, \ \varepsilon_4 = \frac{(\rho C_P)_{nf}}{(\rho C_P)_f}, \ \varepsilon_4 = \frac{\kappa_{nf}}{\kappa_f}$$

Exact solutions

Exact solution for momentum equation.
Consider Eq. (16)'s solution, which has the following structure (See[45])

$$f(\eta) = f_\infty + \left(V_C - f_\infty\right)Exp(-\beta\eta), \tag{20}$$

$$\text{here, } f_\infty = \beta - \frac{Da^{-1}}{\beta}, \tag{21}$$

Although, from the governing B. Cs $f(0) = V_C,\ f_\eta(\infty) = 0,$ and $f_{\eta\eta}(0) = -2(1 + M_a)$ is simultaneously satisfied f_∞ for $\beta > 0$ is as follows

$$f_\infty = V_C + \frac{2(1 + M_a)}{\beta^2}. \tag{22}$$

On applying Eqs. (20, 21) in Eq. (16) to yield the following cubic equation

$$\varepsilon_1\left(1 + \frac{1}{\Lambda}\right)\beta^3 - \varepsilon_2 V_C\beta^2 - \left(\varepsilon_1 Da^{-1} + \varepsilon_3 Q\right)a - 2\varepsilon_2(1 + M_a) = 0. \tag{23}$$

Then the velocity can be required as

$$f_\eta(\eta) = -\beta\left(V_C - f_\infty\right)Exp(-\beta\eta). \tag{24}$$

Exact solution for temperature and concentration equation.
For the purpose of solving temperature and concentration equation we introduce the following new variable for temperature and concertation respectively as follows

$$\xi = \left(\frac{\Pr\left(V_C - f_\infty\right)}{\beta(\varepsilon_5 + R)}\right)Exp(-\beta\eta), \text{ for temperature} \tag{25}$$

$$\varsigma = \left(\frac{Sc\left(V_C - f_\infty\right)}{\beta}\right)Exp(-\beta\eta), \text{ for concentration} \tag{26}$$

Using Eqs. (25) and (26) respectively in Eqs. (17) and (18) to get

$$\xi\frac{\partial^2\theta}{\partial\xi^2} + (1 - \varepsilon_4 S_1 - \varepsilon_4\xi)\frac{\partial\theta}{\partial\xi} + \varepsilon_4\left(2 - \frac{\gamma_1}{\xi}\right)\theta = -Ec_1\xi, \tag{27}$$

$$\varsigma\frac{\partial^2\phi}{\partial\varsigma^2} + \left(1 - p - \varsigma\right)\frac{\partial\phi}{\partial\varsigma} + \left(2 + \frac{q}{\varsigma}\right)\phi = 0, \tag{28}$$

here

$$\begin{aligned}
&S_1 = \frac{\Pr f_\infty}{\beta(\varepsilon_5 + R)}, \quad \gamma_1 = \frac{I\Pr}{\beta(\varepsilon_5 + R)}\\
&Ec_1 = -\frac{Ec\beta^2}{\Pr^2}(\varepsilon_5 + R)\left(\varepsilon_1\beta^2 + \left(\varepsilon_1 Da^{-1} + \varepsilon_3 Q\right)\right)\\
&p = \frac{Scf_\infty}{\beta} \quad q = -\frac{Sc\delta}{\beta^2},
\end{aligned}$$

The B. Cs are also reducing to

$$\theta(\xi = -1) = 1, \quad \theta(\xi = 0) = 0, \tag{29}$$

$$\phi(\varsigma = -1) = 1, \quad \phi(\varsigma = 0) = 0, \tag{30}$$

on solving Eqs. (27) and (28) by using Frobenius method to yield the following equations

$$\theta(\eta) = (1 - A_3)Exp(-\beta A_2\eta)\frac{L(2 - A_2,\ A_1,\ \varepsilon_4\xi)}{L(2 - A_2,\ A_1,\ -\varepsilon_4\xi_0)} + A_3\xi^2, \tag{31}$$

$$\phi(\eta) = Exp(-\beta B_2\eta)\frac{L(2 - B_2,\ B_1,\ \varsigma)}{L(2 - B_2,\ B_1,\ \varsigma_0)}. \tag{32}$$

where

$$A_1 = \sqrt{\varepsilon_4^2 S_1^2 + 4\varepsilon_4\gamma_1}, \quad A_2 = \frac{\varepsilon_4 S_1}{2} + \frac{\sqrt{\varepsilon_4^2 S_1^2 + 4\varepsilon_4\gamma_1}}{2}, \quad A_3 = \frac{\varepsilon_4 Ec_1}{\varepsilon_4(2S_1 + \gamma_1) - 4}$$

$$B_1 = \sqrt{P^2 - 4q}, \quad B_2 = \frac{P}{2} + \frac{\sqrt{P^2 - 4q}}{2}$$

$$\xi_0 = \left(\frac{\Pr\left(V_C - f_\infty\right)}{\beta(\varepsilon_5 + R)}\right), \quad \varsigma_0 = \left(\frac{Sc\left(V_C - f_\infty\right)}{\beta}\right)$$

Results and discussion

This article portrays the Casson fluid flow with Marangoni convection with Carbon nanoparticles are immersed in the fluid flow to enhance the thermal efficiency of the fluid. Analytical results are examined with the help of different controlling parameters namely Casson fluid parameter, inverse Darcy number, Chandrasekhar's number, Marangoni number and so on. The significant effect of Prandtl number, Schmidt number, chemically reaction coefficient and heat source/sink parameter on temperature, concentration and heat source/sink parameter is discussed as follows. The graphical scenario can be disused as follows.

Figure 2a,b demonstrated that the one of the results of Eq. (23), The red solid and dashed lines of the figure represents non-physical solution for various values of Ma and keeping other parameters with suitable values. The effect of the physical solution varied directly with V_C, Da^{-1} and Ma. Similarly, Fig. 3a,b portrays the plots of physical solution verses Ma for different Casson fluid parameter Λ for $V_C > 0$ and $V_C < 0$ cases respectively. Figures 4 and 5 represents the relation associated with velocity $f_\eta(0)$ with roots β_1, β_2 β_3 for various values of Ma. The physical and nonphysical surfaces depending upon the positive and negative roots respectively. From Fig. 4a,b we observe that the Λ directly affected the surface velocity and Ma. Also from Fig. 5a–c it is cleared that the V_C is directly affected the surface velocity and Ma. Figure 6 indicates $f(\eta)$ verses η for different values of Λ. In this Fig. 6a represents suction case, Fig. 6b indicates injection case and Fig. 6c indicates no permeability case. Here it is cleared that $f(\eta)$ is less for more values of Λ for both suction, injection and no permeability cases. Figure 7a–c indicates $f_\eta(\eta)$ verses η for various values of Λ for $V_C > 0$, $V_C < 0$ and $V_C = 0$ respectively. From this it is cleared that $f_\eta(\eta)$ decreases with increasing the values of Λ for $V_C > 0$, $V_C < 0$ and $V_C = 0$.

Impact of $f(\eta)$ verses η and $f_\eta(\eta)$ verses η for various values of M_a is respectively indicated at Fig. 8a,b for $V_C > 0$, and keeping all other parameters with suitable values. Here $f(\eta)$ and $f_\eta(\eta)$ is more for more values of M_a for $V_C > 0$. Figure 9a,b indicates $f(\eta)$ verses η and $f_\eta(\eta)$ verses η for different values of M_a at $V_C < 0$ respectively. Here $f(\eta)$ is more for more values of M_a for injection case. Also $f_\eta(\eta)$ less for more values of M_a for $V_C < 0$. Figure 10a,b portrays the $f(\eta)$ verses η and $f_\eta(\eta)$ verses η for various values of V_C respectively. Here $f(\eta)$ is more for more values of V_C. Also $f_\eta(\eta)$ less for more values of V_C.

The effect of $\theta(\eta)$ on η for various values of Λ, I, and Da^{-1} is respectively represented at Fig. 11a–c. Here, $\theta(\eta)$ more for more values of Λ and Da^{-1}, but $\theta(\eta)$ less for more values of I. And also we observe that after certain values of Λ lines are merging each other. The effect of $\phi(\eta)$ on η for different choices of Sc, δ, and V_C is respectively represented at Fig. 12a–c. from these graphs it is cleared that $\phi(\eta)$ decreases with increasing the values of Sc, δ, and V_C. The inclusion of porous media, heat source/sink parameter, thermal radiation and mass transpiration greatly useful in many fields, porous media prevents heat loss/gain and also accelerates the heat source/sink. Heat source/sink results in thinning of the thermal boundary, Marangoni convection results in more induced flows.

Conclusion

The investigation of results from the 2-D Casson fluid with mass transpiration, thermal radiation and chemically reaction parameter. The ODEs of equations are yielded when we mapped PDEs equation with similarity variables. These ODE equations are solved exactly then the momentum equation is solved to get solution domain, this domain is used in energy and concentration equation to get the temperature profile and concentration profile. The outlook of the present work explains the importance of porous media, thermal radiation, Marangoni convection, thermal radiation and heat source/sink parameter in the physically modelling of the flow. The outcomes we discovered using the graphical scenario are as follows.

1. Effect of the physical solution is directly affected by the V_C, Da^{-1} and Q.
2. Λ and V_C directly affected the surface velocity and Ma.
3. $f(\eta)$ and $f_\eta(\eta)$ decreases for the instance of suction, injection and no permeability case for rising the values of Λ for both suction, injection and no permeability cases.
4. $f(\eta)$ and $f_\eta(\eta)$ more if we rising the values of M_a for suction case.
5. $f(\eta)$ more for more values of M_a for suction case. But $f_\eta(\eta)$ less for more values of M_a for injection case. And $f(\eta)$ more for more values of V_C but $f_\eta(\eta)$ less for more values of V_C.
6. $\theta(\eta)$ more for more values of Λ and Da^{-1}, but $\theta(\eta)$ less for more values of I.
7. $\phi(\eta)$ less for more values of Sc, δ, and V_C.
8. Presence of porous media, prevents heat loss/gain and also accelerates the heat source/sink. Chemical reaction term thinning the thermal boundary, Marangoni convection results in more induced flows.
9. The future perspectives of the present work motivate to explain the physically flow problem on the basis of chemically radiative thermosolutal Marangoni convective fluid also helps to conduct flow problems with porous media.
10. Following conditions explain the comparison pf present work with previous works.

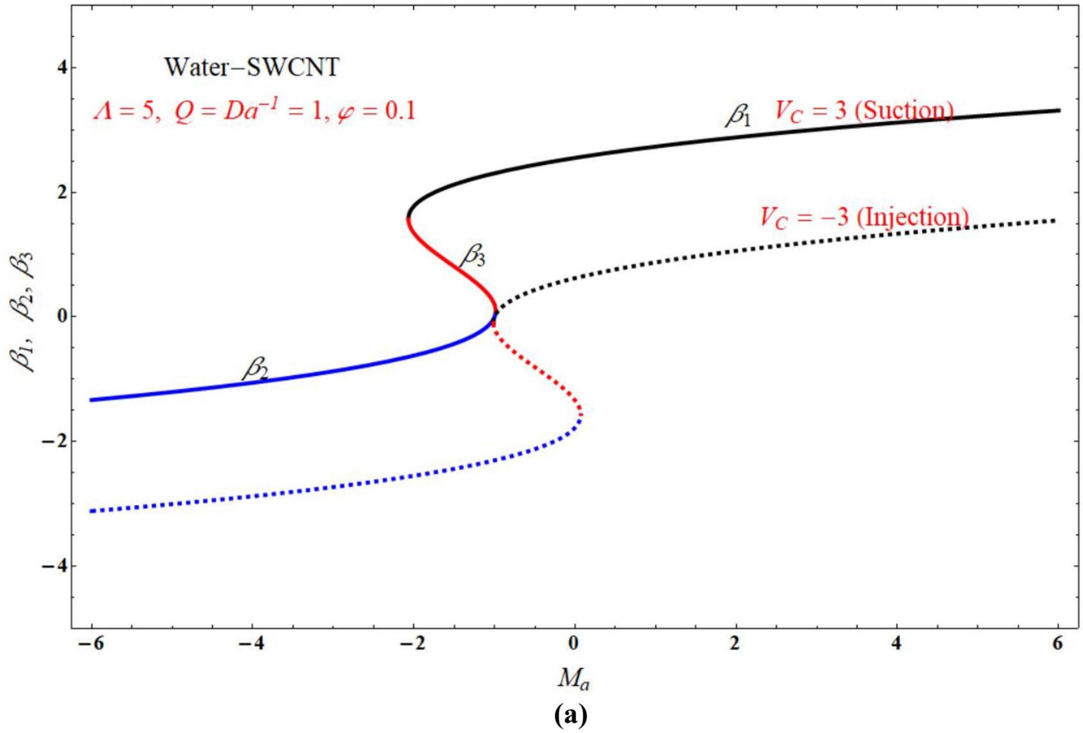

Figure 2. The plots of $\beta_1,\ \beta_2,\ \beta_3$ verses Ma for suction and injection cases at (**a**) $\Lambda = 5$, and (**b**) $\Lambda = 1$.

a. If $Q = \phi = Ec = 0$(In Eqs. 16 and 17)$\Rightarrow$ Mahabaleshwar et al.[33].
b. If $Q = \phi = Ec = R = 0$ (In Eqs. 16 and 17) $\Rightarrow$ Mudhaf and Chamkha[8].
c. If $Q = \phi = Ec = Da^{-1} = 0$ (In Eqs. 16 and 17)$\Rightarrow$ Magyari and Chamkha [14],

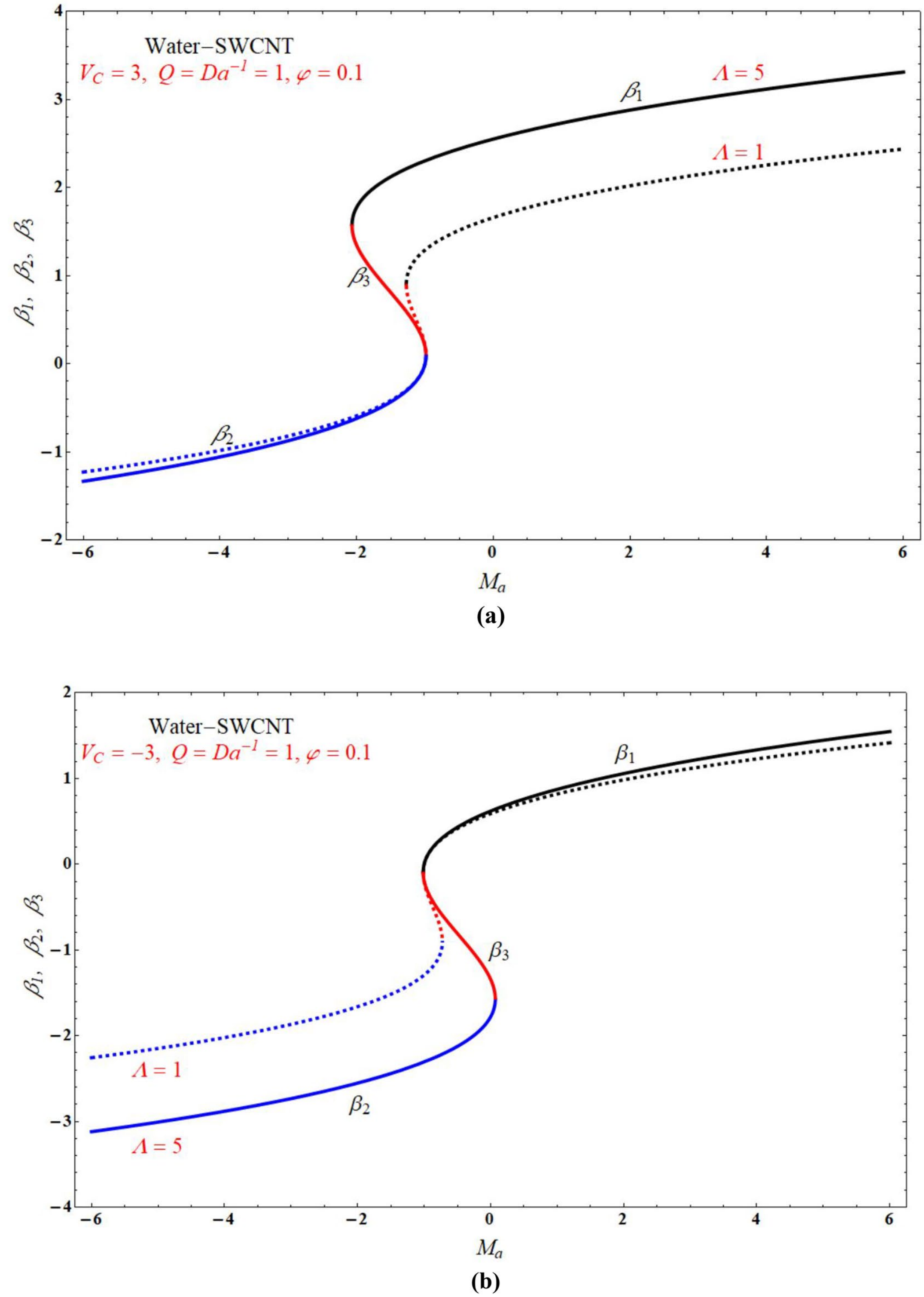

Figure 3. The plots of $\beta_1,\ \beta_2,\ \beta_3$ verses Ma for $\Lambda = 5$ and $\Lambda = 1$ cases at (**a**) $V_C = 3$, and (**b**) $V_C = -3$.

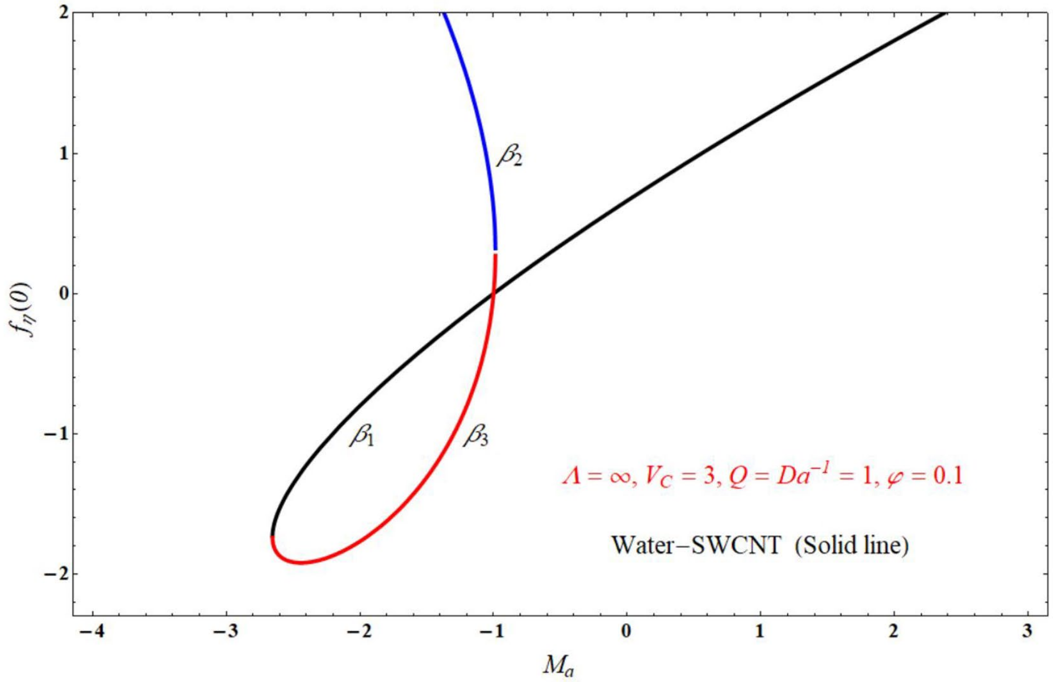

(a)

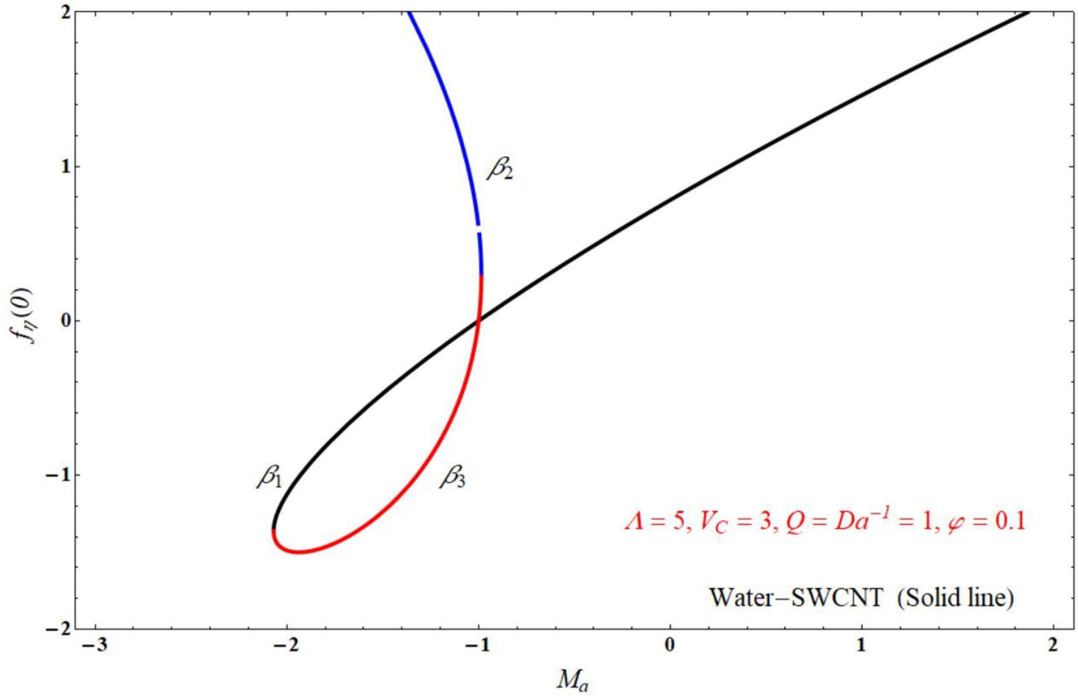

(b)

Figure 4. The plots of $f_\eta(0)$ verses Ma at (a) $\Lambda = \infty$, and (b) $\Lambda = 5$.

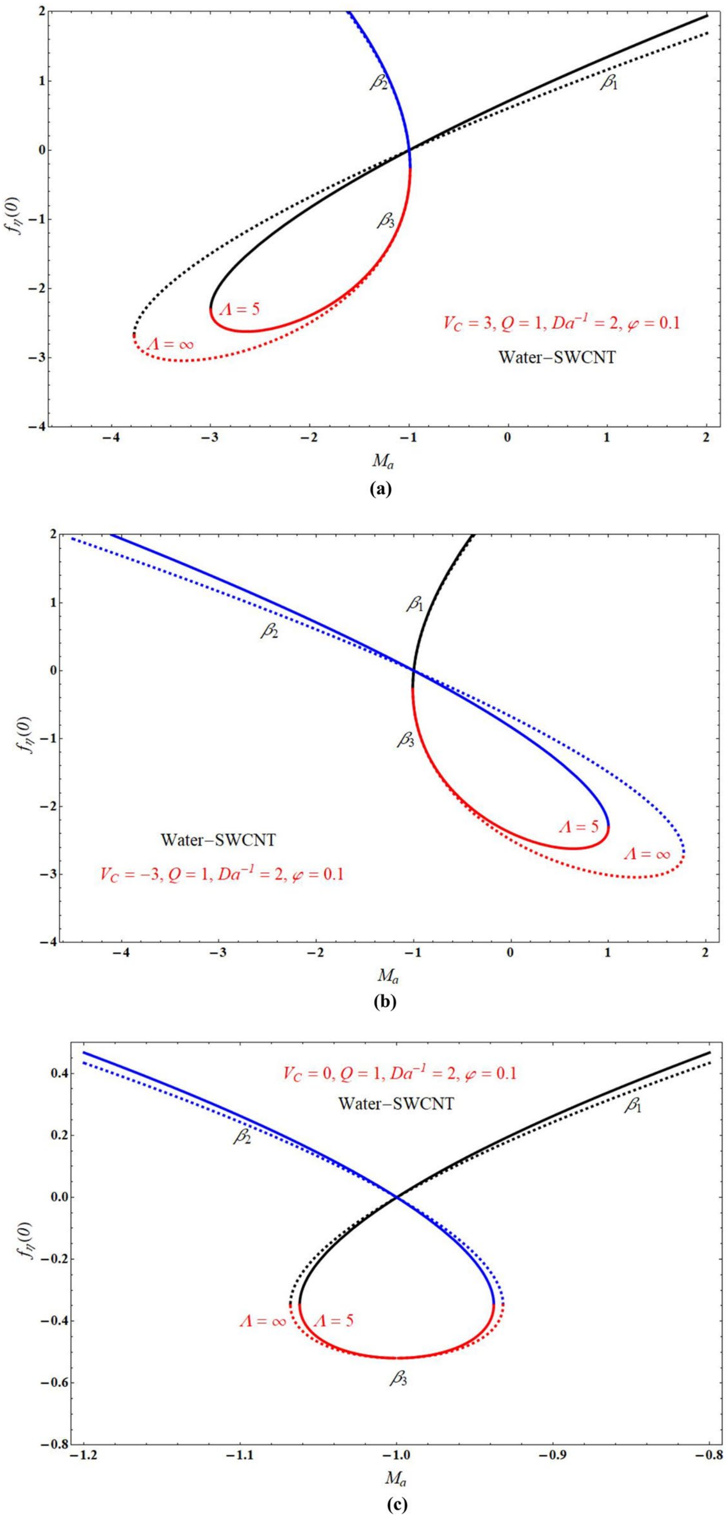

Figure 5. The plots of $f_\eta(0)$ verses Ma for $\Lambda = 5$ and $\Lambda = \infty$ at (**a**) $V_C = 3$, (**b**) $V_C = -3$ and (**c**) $V_C = 0$.

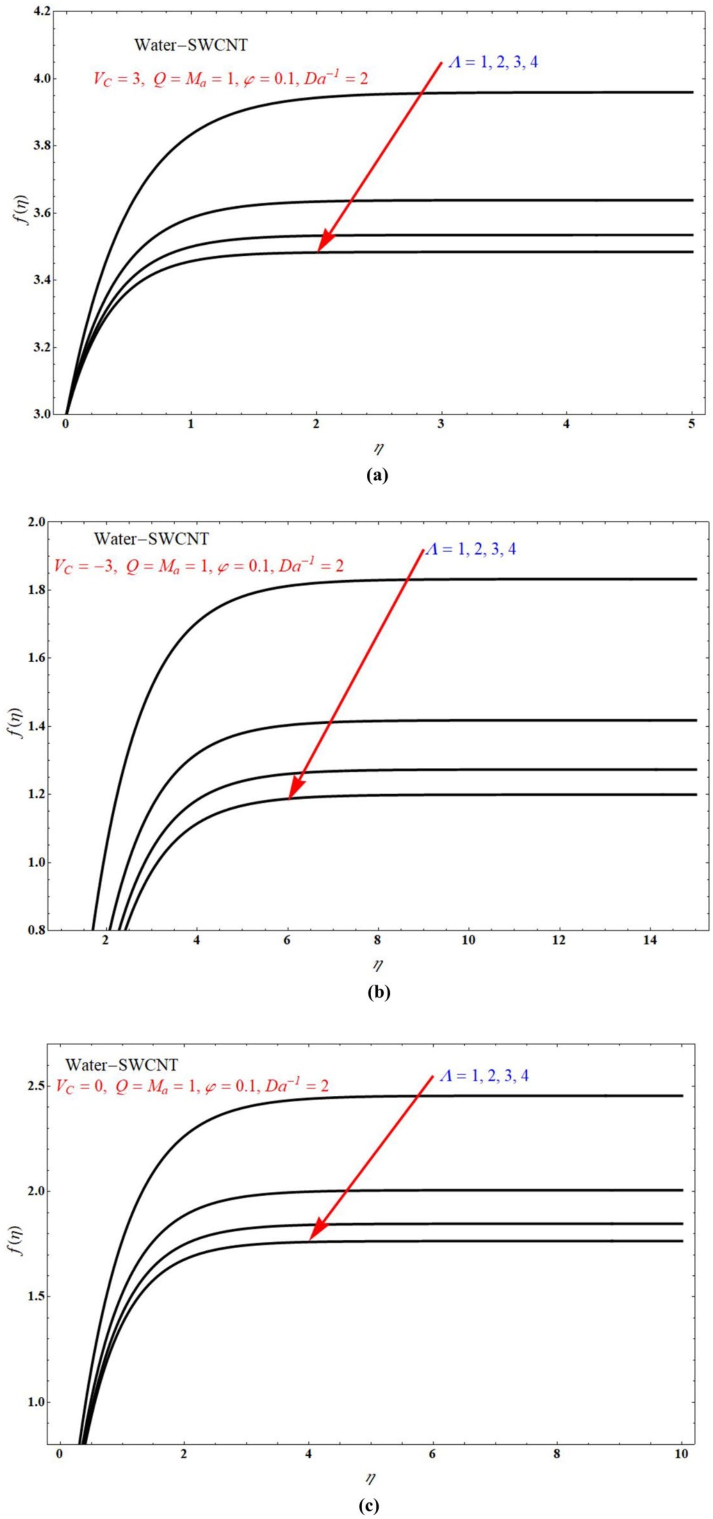

Figure 6. $f(\eta)$ verses η for various values of Λ at (**a**) $V_C = 3$, (**b**) $V_C = -3$ and (**c**) $V_C = 0$.

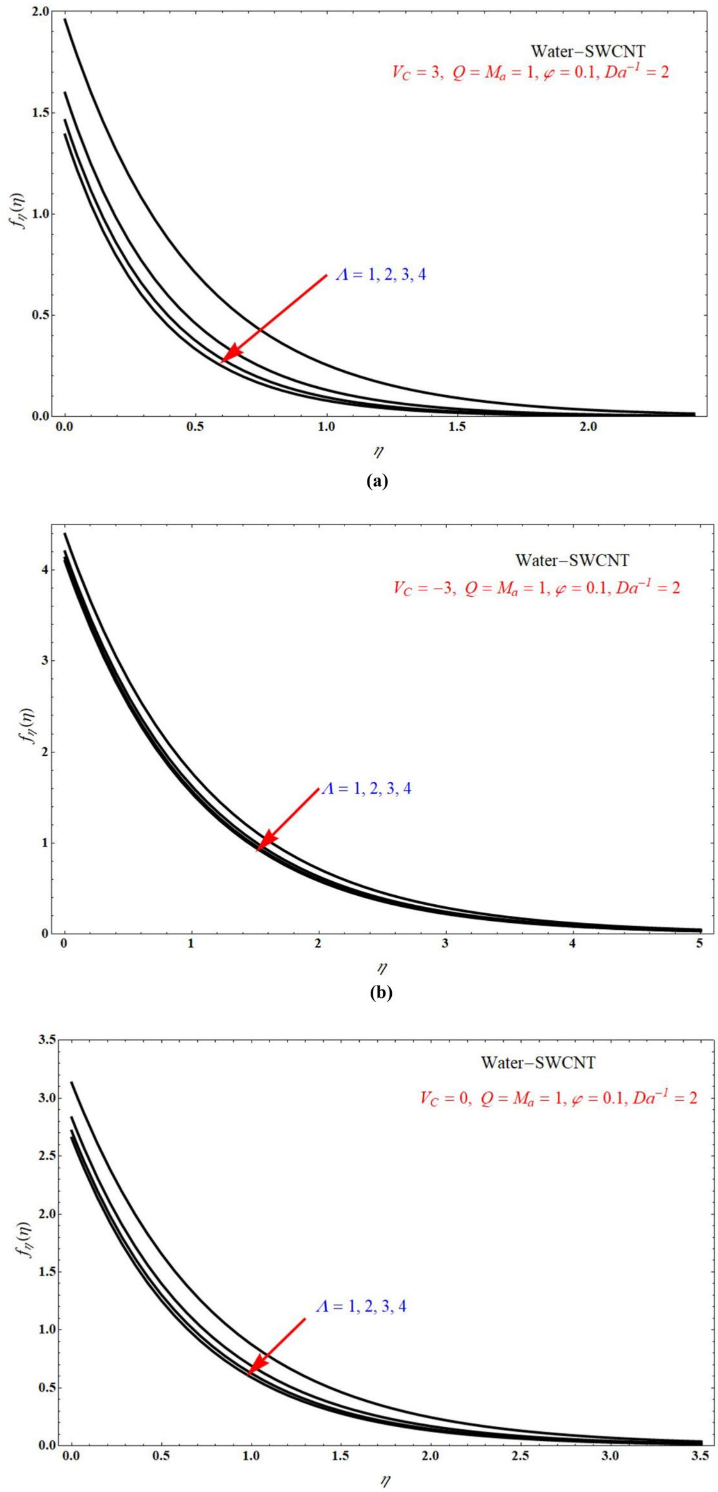

Figure 7. $f_\eta(\eta)$ verses η for various values of Λ at (**a**) $V_C = 3$, (**b**) $V_C = -3$ and (**c**) $V_C = 0$.

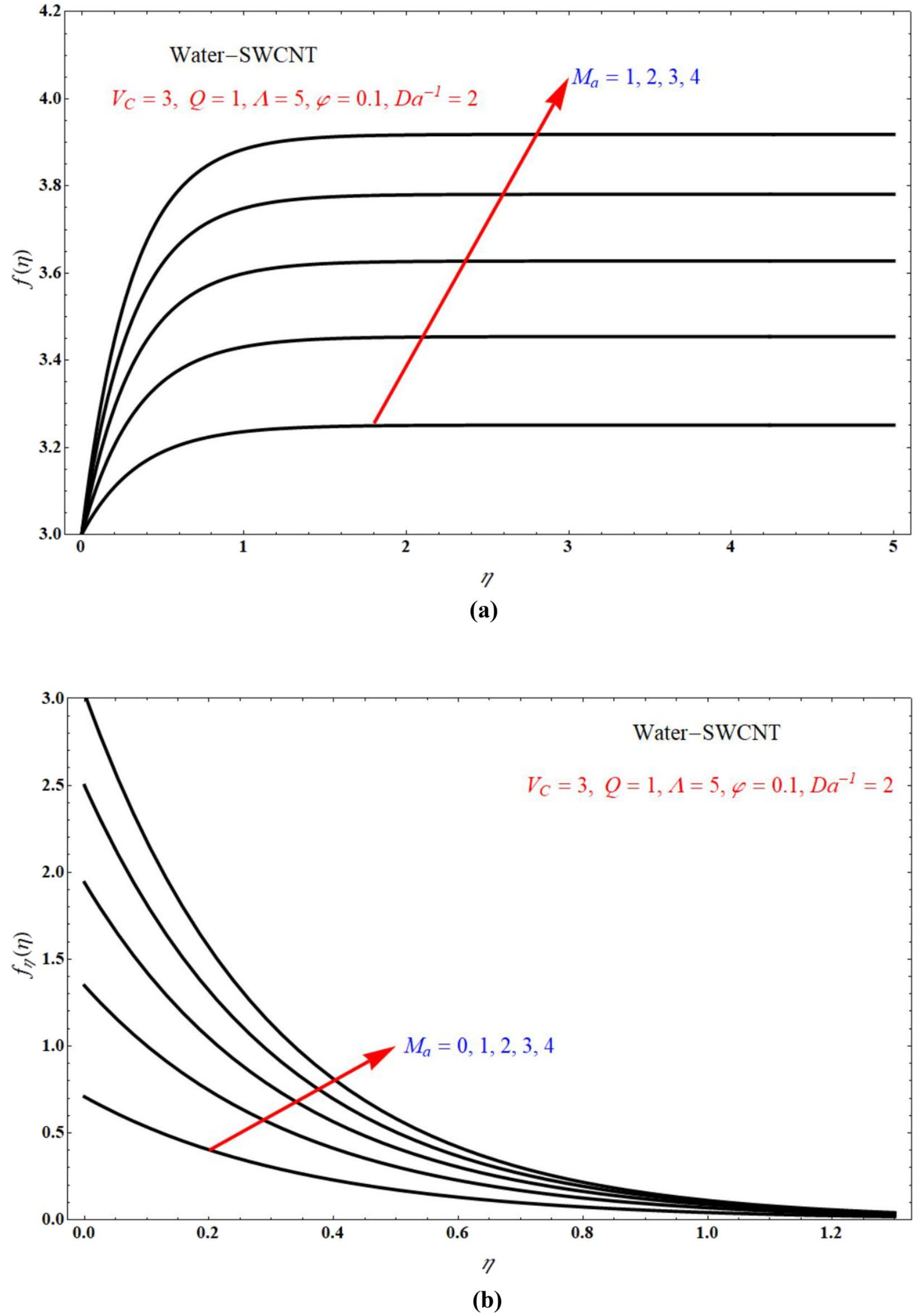

Figure 8. Plots of (**a**) $f(\eta)$ verses η and (**b**) $f_\eta(\eta)$ verses η for different choices of M_a at suction case.

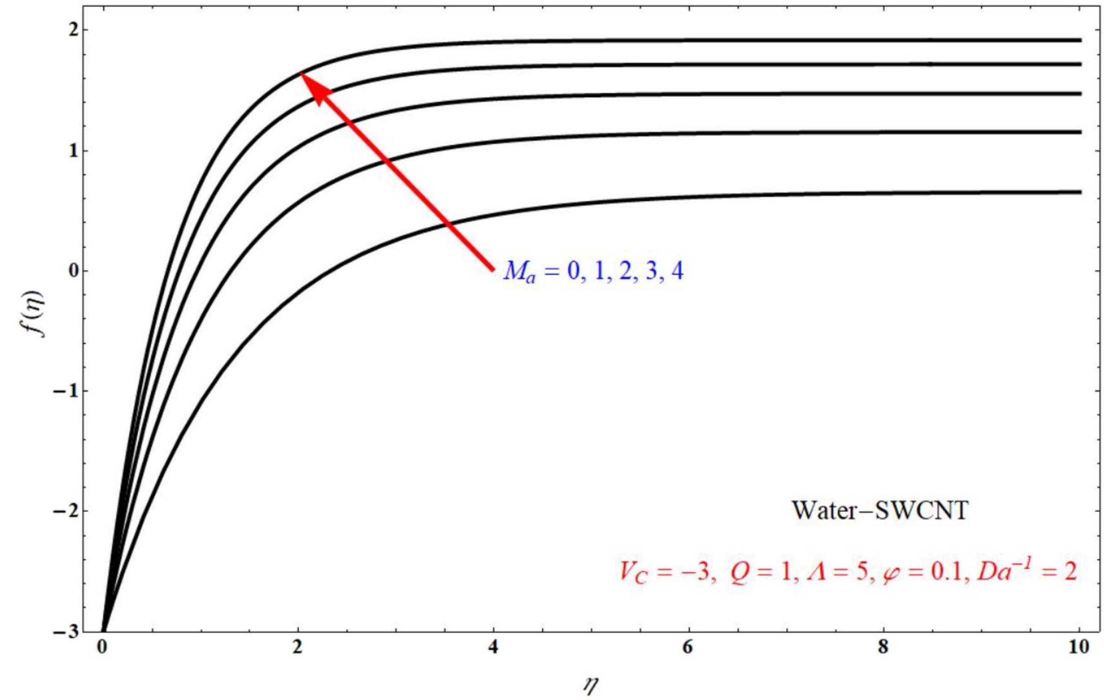

(a)

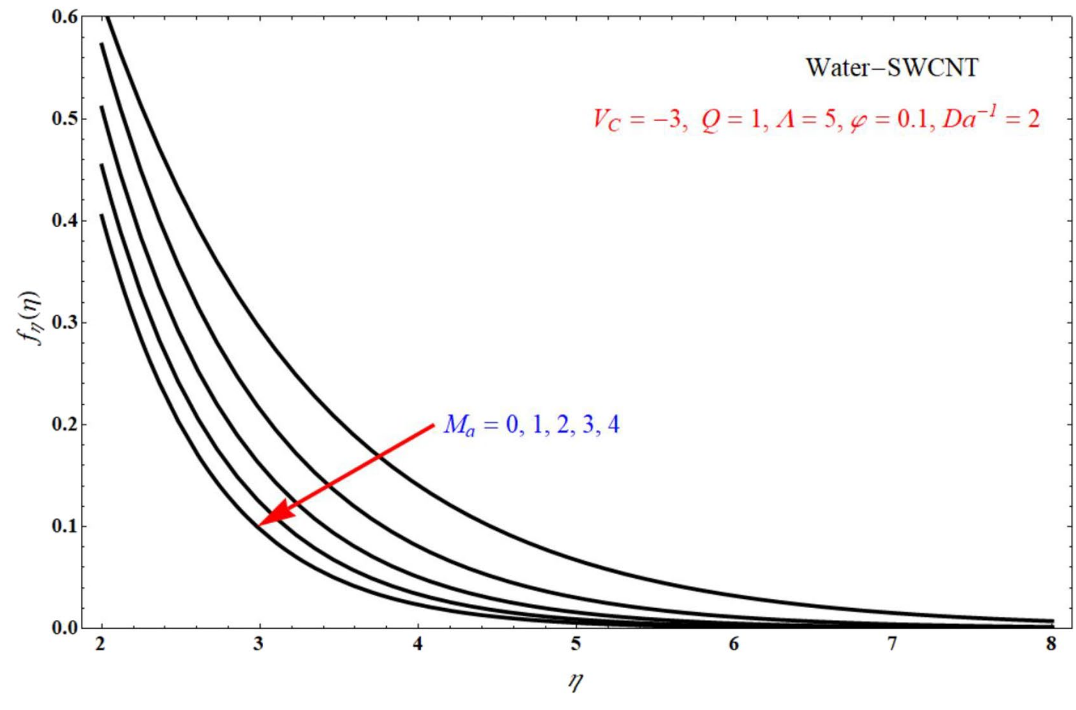

(b)

Figure 9. The plots of (**a**) $f(\eta)$ verses η and (**b**) $f_\eta(\eta)$ verses η for different choices of M_a at injection case.

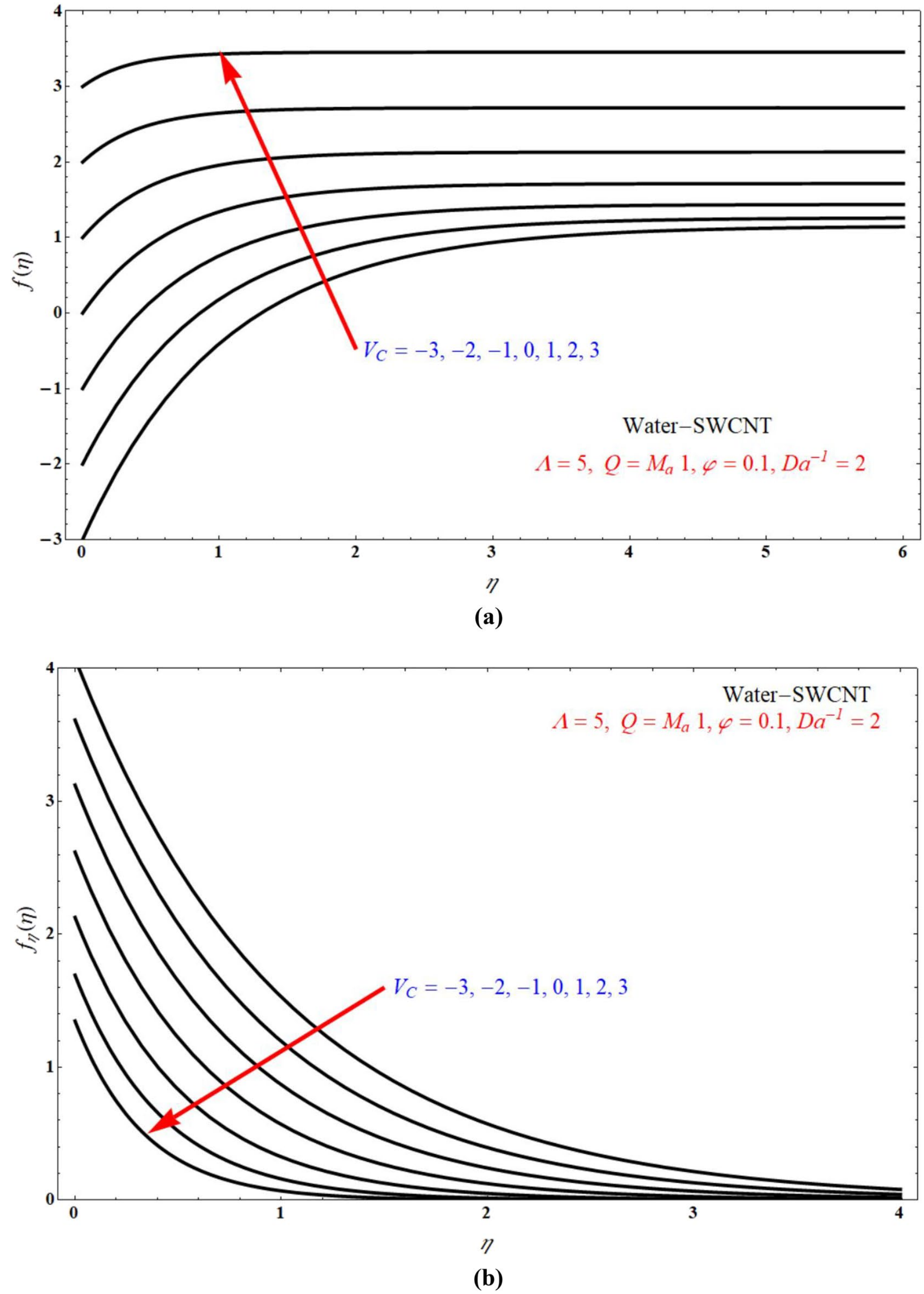

Figure 10. The plots of (**a**) $f(\eta)$ verses η and (**b**) $f_\eta(\eta)$ verses η for different choices of V_C.

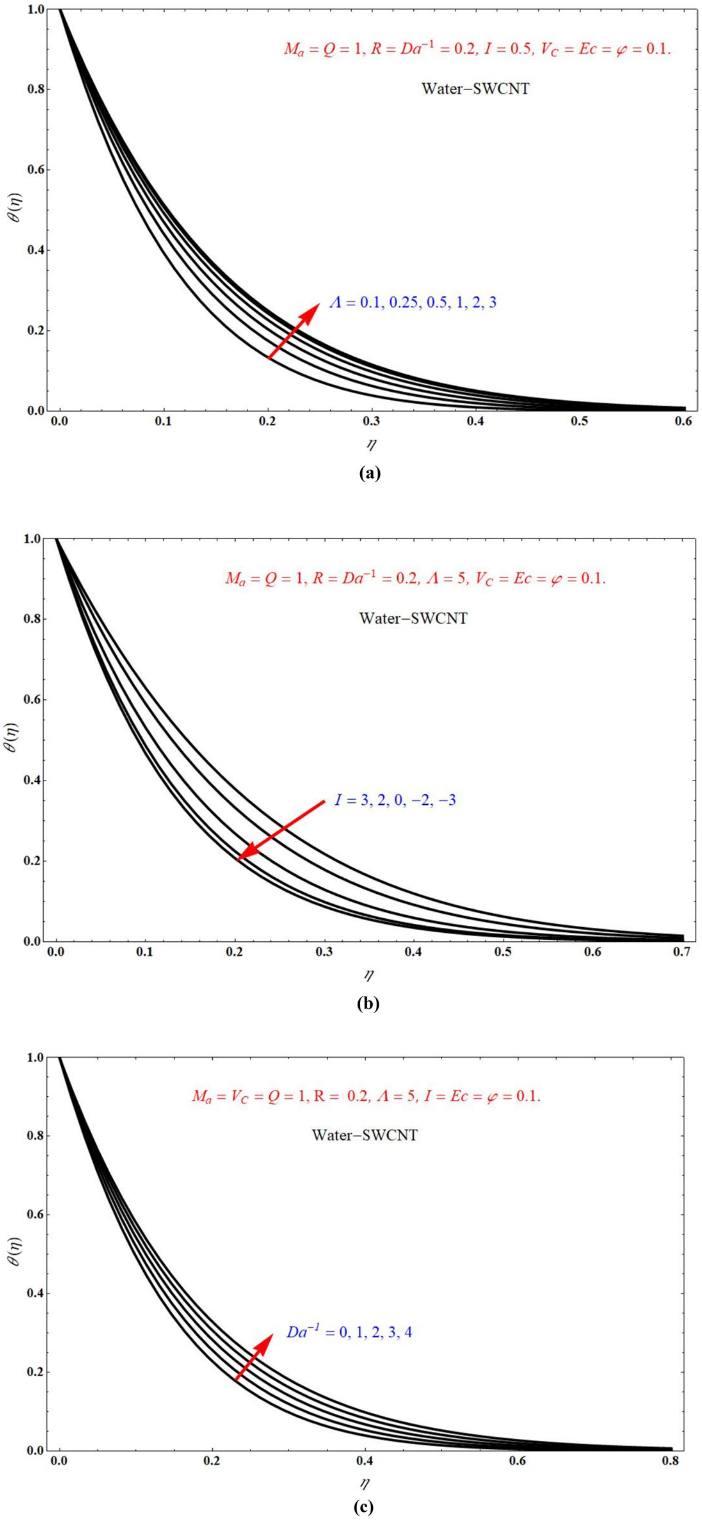

Figure 11. $\theta(\eta)$ verses η for various values of (**a**) Λ (**b**) I and (**c**) Da^{-1}.

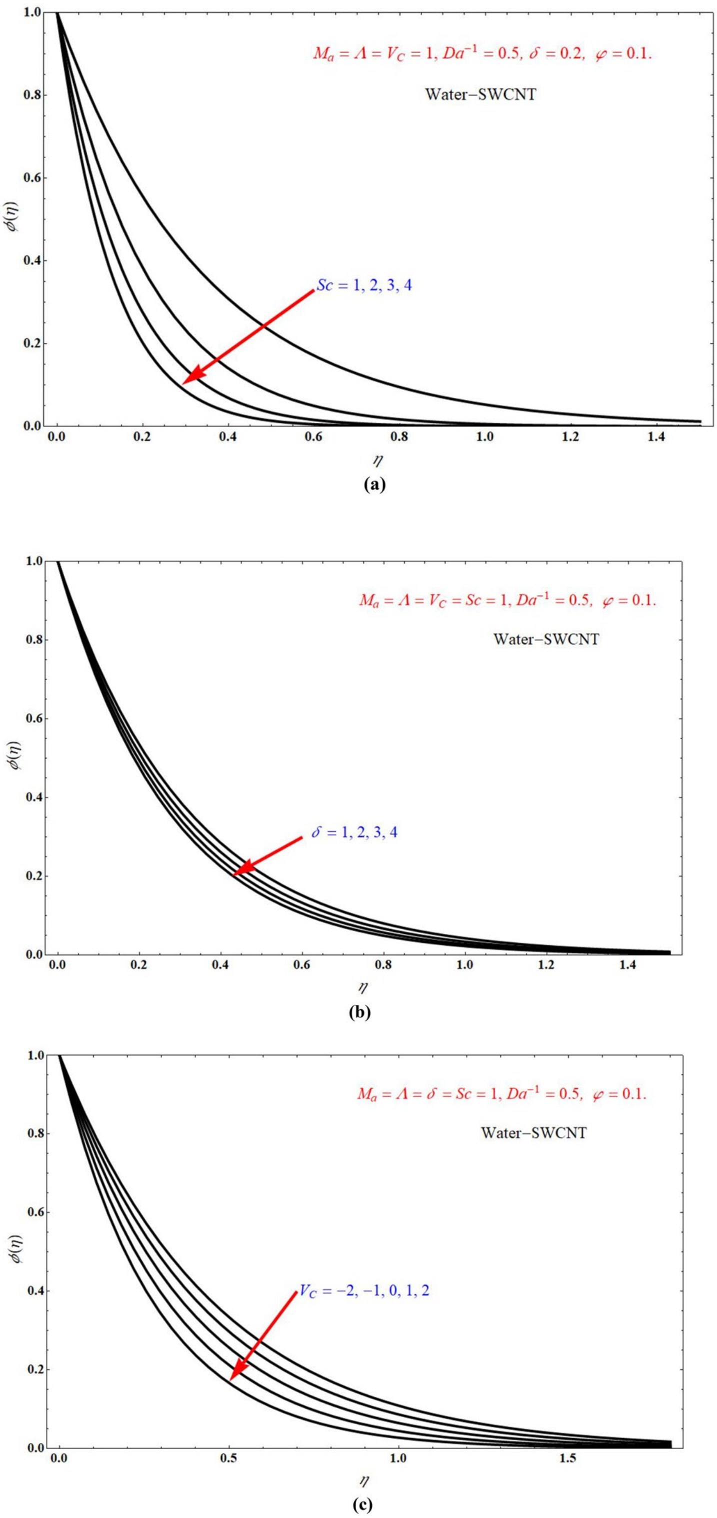

Figure 12. The plots of $\phi(\eta)$ verses η for different choices of (**a**) Sc (**b**) δ and (**c**) V_C.

Data availability

The datasets used and/or analysed during the current study available from the corresponding author on reasonable request.

Received: 6 July 2022; Accepted: 14 September 2022
Published online: 27 September 2022

References

1. Gibbs, J. W. On the equilibrium of heterogeneous substances: Part II. *Trans. Conn. Acad. Arts Sci.* **3**, 343–524 (1878).
2. Napolitano, L.G. Microgravity fluid dynamics. In *2nd Levitch Conference*, Washington, (1978).
3. Napolitano, L.G. Marangoni boundary layers. In *Proceedings of the 3rd European Symposium on Material Science in Space*. Grenoble, ESA SP-142, (1979).
4. Lin, Y. H., Zheng, L. C. & Zhang, X. X. Magnetohydrodynamics thermo capillary Marangoni convection heat transfer of power-law fluids driven by temperature gradient. *ASME J. Heat Transf.* **135**(5), 051702 (2013).
5. Lin, Y., Zheng, L. & Zhang, X. Radiation effects on Marangoni convection flow and heat transfer in pseudo-plastic non-Newtonian nanofluids with variable thermal conductivity. *Int. J. Heat Mass Transf.* **77**, 708–716 (2014).
6. Chamkha, A. J., Pop, I. & Takhar, H. S. Marangoni mixed convection boundary layer flow. *Meccanica* **41**, 219–232 (2006).
7. Napolitano, L. G. Surface and buoyancy driven free convection. *Acta Astronaut.* **9**, 199–215 (1982).
8. Mudhaf, A. A. & Chamkha, A. J. Similarity solutions for MHD thermosolutal Marangoni convection over a flat surface in the presence of heat generation or absorption effects. *Heat Mass Transf.* **42**, 112–121 (2005).
9. Aly, E. H. & Ebaid, A. Exact analysis for the effect of heat transfer on MHD and radiation Marangoni boundary layer nanofluid flow past a surface embedded in a porous medium. *J. Mol. Liq.* **215**, 625–639 (2016).
10. Arbin, N., Saleh, H., Hashim, J. & Chamkha, A. J. Numerical investigation of double-diffusive convection in an open cavity with partially heated wall via heatline approach. *Int. J. Therm. Sci.* **100**, 169–184 (2016).
11. Nayak, M. K. Chemical reaction effect on MHD viscoelastic fluid over a stretching sheet through porous medium. *Meccanica* **56**, 1699 (2016).
12. Dandapat, B. S. & Kumar, B. P. Onset of thermosolutal convection in a liquid layer having deformable free surface: I—Stationary convection. *Z. Naturforsch.* **47**, 554–560 (1992).
13. Magyari, E. & Chamkha, A. J. Combined effect of heat generation or absorption and first-order chemical reaction on micropolar fluid flows over a uniformly stretched permeable surface: The full analytical solution. *Int. J. Therm. Sci.* **49**, 1821–1828 (2010).
14. Magyari, E. & Chamkha, A. J. Exact analytical results for the thermosolutal MHD Marangoni boundary layers. *Int. J. Therm. Sci.* **47**, 848 (2008).
15. Mahanthesh, B. & Gireesha, B. J. Thermal Marangoni convection in two-phase flow of dusty Casson fluid. *Results Phys.* **8**, 537–544 (2018).
16. Choi, S. U. S., Eastman, J.A. Enhancing thermal conductivity of fluids with nanoparticles, No. ANL/MSD/CP-84938, CONF-951135-29, Argonne National Lab., IL, USA, (1995).
17. Khan, A., Shah, Z., Alzahrani, E. & Islam, S. Entropy generation and thermal analysis for rotary motion of hydro magnetic Casson nanofluid past a rotating cylinder with Joule heating effect. *Int. Comm. Heat and Mass Transf.* **119**, 104979 (2020).
18. Khan, A. *et al.* Bio-convective and chemically reactive hybrid nanofluid flow upon a thin stirring needle with viscous dissipation. *Sci. Rep.* **11**, 8066 (2021).
19. Khan, A. *et al.* Bio-convective micropolar nanofluid flow over thin moving needle subject to Arrhenius activation energy, viscous dissipation and binary chemical reaction. *Case Stud. Thermal Eng.* **25**, 100989 (2021).
20. Khan, A. *et al.* Chemically reactive nanofluid flow past a thin moving needle with viscous dissipation, magnetic effects and hall current. *PLoS ONE* **16**(4), e0249264 (2021).
21. Islam, S. *et al.* Radiative mixed convection flow of Maxwell nanofluid over a stretching cylinder with joule heating and heat source/sink effects. *Sci. Rep.* **10**, 17823 (2020).
22. Khan, A. *et al.* Radiative Swirl motion of hydromagnetic Casson nanofluid flow over rotary cylinder using Joule dissipation impact. *Phys. Scr.* **96**(4), 045206 (2021).
23. Mahabaleshwar, U. S., Sneha, K. N. & Huang, H.-N. An effect of MHD and radiation on CNTS-Water based nanofluids due to a stretching sheet in a Newtonian fluid. *Case Stud. Therm. Eng.* **28**, 101462 (2021).
24. Khan, A. *et al.* Darcy-Forchheimer flow of MHD CNTs nanofluid radiative thermal behavior and convective non uniform heat source/sink in the rotating frame with microstructure and inertial characteristics. *AIP Adv.* **8**(12), 125024 (2018).
25. Khan, W. A., Khan, Z. H. & Rahi, M. Fluid flow and heat transfer of carbon nanotubes along a flat plate with Navier slip boundary. *Appl. Nanosci.* **4**, 633–641 (2014).
26. Raju Chakravarthala, S. K., Sandeep, N., Ali, M. E. & Nuhait, A. O. Heat and mass transfer in 3-D NHD Williamson-Casson fluids flow over a stretching surface with non-uniform heat source/sink. *Therm. Sci.* **23**, 281–293 (2019).
27. Kumaran, G., Sandeep, N. & Ali, M. E. Computational analysis of magnetohydrodynamic Casson and Maxwell flows over a stretching sheet with cross diffusion. *Results Phys.* **7**, 147–155 (2017).
28. Ali, M. E. & Sandeep, N. Cattaneo-Christov model for radiative heat transfer of magnetohydrodynamic Casson-ferrofluids: A numerical study. *Results Phys.* **7**, 21–30 (2017).
29. Fisher, B. G. *Extrusion of Plastics* (Newnes-Butterworld, 1976).
30. Aly, E. H. & Vajravelu, K. Exact and numerical solutions of MHD nano boundary layer flows over stretching surfaces in porous medium. *Appl. Math. Comput.* **232**, 191–240 (2014).
31. Sreedevi, P., Reddy, P. S. & Chamkha, A. J. Heat and Mass transfer analysis of nanofluid over linear and non-linear stretching surfaces with thermal radiation and chemical reaction. *Powder Tech.* **315**, 194–204 (2017).
32. Nayak, M. K., Akbar, N. S., Pandey, V. S., Khan, Z. H. & Tripathis, D. 3D free convective MHD flow of nanofluid over permeable linear stretching sheet with thermal radiation. *Powder Tech.* **315**, 205–215 (2017).
33. Mahabaleshwar, U. S., Nagaraju, K. R., Vinay Kumar, P. N. & Azese, M. N. Effect of radiation on thermosolutal Marangoni convection in a porous medium with chemical reaction and heat source/sink. *Phys. Fluids* **32**, 106602 (2020).
34. Aly, E. H. Dual exact solutions of graphene-water nanofluid flow over stretching/shrinking sheet with suction/injection and heat source/sink: Critical values and regions with stability. *Powder Tech.* **342**, 528–544 (2019).
35. Mahabaleshwar, U. S., Aly, E. H. & Vishalakshi, A. B. MHD and thermal radiation flow of graphene casson nanofluid stretching/shrinking sheet. *Int. J. Appl. Comput. Math.* **8**, 113 (2022).
36. Ganesh Kumar, K., Gireesha, B. J., Prasannakumara, B. C. & Makinde, O. D. Impact of chemical reaction on marangoni boundary layer flow of a casson nano liquid in the presence of uniform heat source sink. *Diffus. Found.* **11**, 22–32 (2017).
37. Zhang, Y. & Zheng, L. Analysis of MHD thermosolutal Marangoni convection with the heat generation and a first-order chemical reaction. *Chem. Eng. Sci.* **69**, 449–455 (2012).
38. Lin, Y. & Zheng, L. Marangoni boundary layer flow and heat transfer of copper-water nanofluid over a porous medium disk. *AIP Adv.* **5**, 107225 (2015).

39. Cortell, R. Radiation effects for the Blasius and sakiadis flows with a convective surface boundary condition. *Appl. Math. Comput.* **206**, 832–840 (2008).
40. Nandy, S. K. & Pop, I. Effects of magnetic field and thermal radiation on stagnation flow and heat transfer of nanofluid over a shrinking surface. *Int. Commun. Heat mass Tranf.* **53**, 50–55 (2014).
41. Siddheshwar, P. G. & Mahabaleshwar, U. S. Effects of radiation and heat source on MHD flow of a viscoelastic liquid and heat transfer over a stretching sheet. *Int. J. Non-Linear Mech.* **40**, 807–820 (2005).
42. Aly, E. H. Existence of the multiple exact solutions for nanofluids flow over a stretching/shrinking sheet embedded in a porous medium at the presence of magnetic field with electrical conductivity and thermal radiation effects. *Powder Tech.* **301**, 760–781 (2016).
43. Anuar, N. S., Bachok, N., Turkyilmazoglu, M., Arfin, N. D. & Rosali, H. Analytical and stability analysis of MHD flow past a nonlinearly deforming vertical surface in carbon nanotubes. *Alex. Eng. J.* **59**, 497–507 (2020).
44. Khalid, A., Khan, I., Khan, A., Shafie, S. & Tlili, I. Case study of MHD blood flow in a porous medium with CNTS and thermal analysis. *Case Stud. Therm. Eng.* **12**, 374–380 (2018).
45. Mahabaleshwar, U. S., Vishalakshi, A. B. & Andersson, H. I. Hybrid nanofluid flow past a stretching/shrinking sheet with thermal radiation and mass transpiration. *Chin. J. Phys.* **75**, 152–168 (2022).

Author contributions

All authors participated in all sections of numerical modeling, results and analysis.

Competing interests

The authors declare no competing interests.

Additional information

Correspondence and requests for materials should be addressed to M.H.

Reprints and permissions information is available at www.nature.com/reprints.

Publisher's note Springer Nature remains neutral with regard to jurisdictional claims in published maps and institutional affiliations.

Open Access This article is licensed under a Creative Commons Attribution 4.0 International License, which permits use, sharing, adaptation, distribution and reproduction in any medium or format, as long as you give appropriate credit to the original author(s) and the source, provide a link to the Creative Commons licence, and indicate if changes were made. The images or other third party material in this article are included in the article's Creative Commons licence, unless indicated otherwise in a credit line to the material. If material is not included in the article's Creative Commons licence and your intended use is not permitted by statutory regulation or exceeds the permitted use, you will need to obtain permission directly from the copyright holder. To view a copy of this licence, visit http://creativecommons.org/licenses/by/4.0/.

© The Author(s) 2022